

Dual programmed cell death pathways induced by p53 transactivation overcome resistance to oncolytic adenovirus in human osteosarcoma cells

Joe Hasei¹, Tsuyoshi Sasaki¹, Hiroshi Tazawa^{2,3}, Shuhei Osaki¹, Yasuaki Yamakawa¹,
Toshiyuki Kunisada^{1,4}, Aki Yoshida¹, Yuuri Hashimoto³, Teppei Onishi³,
Futoshi Uno³, Shunsuke Kagawa³, Yasuo Urata⁵,
Toshifumi Ozaki¹ and Toshiyoshi Fujiwara³

¹Department of Orthopaedic Surgery, Okayama University Graduate School of
Medicine, Dentistry and Pharmaceutical Sciences, Okayama 700-8558, Japan

²Center for Innovative Clinical Medicine, Okayama University Hospital, Okayama
700-8558, Japan

³Department of Gastroenterological Surgery, Okayama University Graduate School of
Medicine, Dentistry and Pharmaceutical Sciences, Okayama 700-8558, Japan

⁴Department of Medical Materials for Musculoskeletal Reconstruction, Okayama
University Graduate School of Medicine, Dentistry and Pharmaceutical Sciences,
Okayama 700-8558, Japan

⁵Oncolys BioPharma, Inc., Tokyo 105-0001, Japan

Running title: p53-mediated dual cell death pathways

Disclosure of Potential Conflict of Interest

Y. Urata is President & CEO of Oncolys BioPharma, Inc., the manufacturer of OBP-301 (Telomelysin). H. Tazawa and T. Fujiwara are consultants of Oncolys BioPharma, Inc. The other authors disclosed no potential conflicts of interest.

Footnotes:

Corresponding Author: Toshiyoshi Fujiwara

Department of Gastroenterological Surgery

Okayama University Graduate School of Medicine, Dentistry and Pharmaceutical Sciences

2-5-1 Shikata-cho, Kita-ku, Okayama 700-8558, Japan

Tel: +81-86-235-7257; Fax: +81-86-221-8775; E-mail: toshi_f@md.okayama-u.ac.jp

Abbreviations: hTERT, human telomerase reverse transcriptase; MOI, multiplicity of infection; PFU, plaque-forming units; ID₅₀, 50% inhibiting doses; GFP, green fluorescent protein; PARP, poly (ADP-ribose) polymerase; LC3, microtubule-associated protein 1 light chain 3; DRAM, damage-regulated autophagy modulator; RT-PCR, reverse transcription-polymerase chain reaction; Ct, threshold cycle; PBS, phosphate buffered saline; 3D-CT, three-dimensional computed tomography; miRNA, microRNA; EGFR, epidermal growth factor receptor.

Grant support: This study was supported by grants-in-aid from the Ministry of Education, Science, and Culture, Japan (T. Fujiwara) and grants from the Ministry of Health and Welfare, Japan (T. Fujiwara), and in part by the National Cancer Center Research and Development Fund (23-A-10) (T. Ozaki).

Word counts: 5499 words (excluding references)

Abstract

Tumor suppressor p53 is a multifunctional transcription factor that regulates diverse cell fates, including apoptosis and autophagy in tumor biology. p53 overexpression enhances the antitumor activity of oncolytic adenoviruses; however, the molecular mechanism of this occurrence remains unclear. We previously developed a tumor-specific replication-competent oncolytic adenovirus, OBP-301, that kills human osteosarcoma cells, but some human osteosarcoma cells were OBP-301-resistant. In this study, we investigated the antitumor activity of a p53-expressing oncolytic adenovirus, OBP-702, and the molecular mechanism of the p53-mediated cell death pathway in OBP-301-resistant human osteosarcoma cells. The cytopathic activity of OBP-702 was examined in OBP-301-sensitive (U2OS and HOS) and OBP-301-resistant (SaOS-2 and MNNG/HOS) human osteosarcoma cells. The molecular mechanism in the OBP-702-mediated induction of two cell death pathways, apoptosis and autophagy, was investigated in OBP-301-resistant osteosarcoma cells. The antitumor effect of OBP-702 was further assessed using an orthotopic OBP-301-resistant MNNG/HOS osteosarcoma xenograft tumor model. OBP-702 suppressed the viability of OBP-301-sensitive and OBP-301-resistant osteosarcoma cells more efficiently than OBP-301 or a

replication-deficient p53-expressing adenovirus (Ad-p53). OBP-702 induced more profound apoptosis and autophagy when compared with OBP-301 or Ad-p53. E1A-mediated *miR-93/106b* upregulation induced p21 suppression, leading to p53-mediated apoptosis and autophagy in OBP-702-infected cells. p53 overexpression enhanced adenovirus-mediated autophagy through activation of damage-regulated autophagy modulator (DRAM). Moreover, OBP-702 suppressed tumor growth in an orthotopic OBP-301-resistant MNNG/HOS xenograft tumor model. These results suggest that OBP-702-mediated p53 transactivation is a promising antitumor strategy to induce dual apoptotic and autophagic cell death pathways via regulation of miRNA and DRAM in human osteosarcoma cells.

Key words: oncolytic adenovirus; telomerase; p53; apoptosis; autophagy

Introduction

Osteosarcoma is one of the most common malignant tumors in young children (1, 2). Current treatment strategies, which consist of multi-agent chemotherapy and aggressive surgery, have significantly improved the cure rate and prognosis of patients with osteosarcoma. In fact, over the past 30 years, the 5-year survival rate has increased from 10% to 70% (3-5). Even in osteosarcoma patients with metastases at diagnosis, the 5-year survival rate has reached 20% to 30% in response to chemotherapy and surgical removal of primary and metastatic tumors (6). However, treatment outcomes for patients with osteosarcomas have further improved over the last few years. Therefore, the development of novel therapeutic strategies is required to improve the clinical outcomes in patients with osteosarcomas.

Tumor-specific replication-competent oncolytic viruses are being developed as novel anticancer therapy, in which the promoters of cancer-related genes are used to regulate virus replication in a tumor-dependent manner. More than 85% of all human cancers express high telomerase activity to maintain the length of the telomeres during cell division, while normal somatic cells seldom show this enhance telomerase activity (7, 8). Telomerase activity has also been detected in 44% to 81% of bone and soft tissue

sarcomas (9, 10). Telomerase activation is closely correlated with the expression of the human telomerase reverse transcriptase (*hTERT*) gene (11). Based on these data, we previously developed a telomerase-specific replication-competent oncolytic adenovirus OBP-301 (Telomelysin), in which the *hTERT* gene promoter drives the expression of the *E1A* and *E1B* genes (12). A phase I clinical trial of OBP-301, which was conducted in the United States on patients with advanced solid tumors, indicated that OBP-301 was well tolerated by patients (13). Recently, we reported that OBP-301 efficiently killed human bone and soft tissue sarcoma cells (14, 15). However, some osteosarcoma cell lines were not sensitive to the antitumor effect of OBP-301. Therefore, to efficiently eliminate tumor cells with OBP-301, its antitumor effects need to be enhanced.

Cancer gene therapy is defined as the treatment of malignant tumors via the introduction of a therapeutic tumor suppressor gene or the abrogation of an oncogene. The tumor-suppressor *p53* gene has an attractive tumor suppressor profile as a potent therapeutic transgene for induction of cell cycle arrest, senescence, apoptosis and autophagy (16). Dual cell death pathways, such as apoptosis and autophagy, induced by *p53* transactivation are mainly involved in the suppression of tumor initiation and progression. However, among the *p53*-downstream target genes, *p21*, which is most rapidly and strongly induced during the DNA damage response, mainly induces cell

cycle arrest through suppression of apoptotic and autophagic cell death pathways (17, 18). Thus, p21 suppression may be a more effective strategy for the induction of apoptotic and autophagic cell death pathways in tumor cells, particularly when the tumor-suppressor *p53* gene is overexpressed in tumor cells in response to cancer gene therapy.

A p53-expressing replication-deficient adenovirus (Ad-p53, Advexin) has previously been reported to induce an antitumor effect in the *in vitro* and *in vivo* settings (19, 20) as well as in some clinical studies (21-24). We recently reported that combination therapy with OBP-301 and Ad-p53 resulted in a more profound antitumor effect when compared to monotherapy with either OBP-301 or Ad-p53 (25). Moreover, we generated armed OBP-301 expressing the wild-type *p53* tumor suppressor gene (OBP-702) and showed that OBP-702 suppressed the viability of various types of epithelial malignant cells more efficiently than did OBP-301 (26). OBP-702 induced a more profound apoptotic cell death effect when compared to Ad-p53, likely via adenoviral E1A-mediated suppression of anti-apoptotic p21 in human epithelial malignant cells. However, it remained unclear whether OBP-702 efficiently induces an antitumor effect in human non-epithelial malignant cells, including osteosarcomas.

In the present study, we investigated the *in vitro* cytopathic efficacy of the

p53-expressing telomerase-specific replication-competent oncolytic adenovirus, OBP-702, in human osteosarcoma cells, and we compared the induction level of apoptotic and autophagic cell deaths in OBP-301-resistant human osteosarcoma cells infected with OBP-301, OBP-702 and Ad-p53. The molecular mechanism by which OBP-702 mediates induction of apoptosis and autophagy was also investigated. Finally, the *in vivo* antitumor effect of OBP-702 was evaluated using an orthotopic OBP-301-resistant human osteosarcoma xenograft tumor model.

Materials and Methods

Cell lines

The human osteosarcoma cell lines, HOS and SaOS-2, were kindly provided by Dr. Satoru Kyo (Kanazawa University, Ishikawa, Japan). These cells were propagated as monolayer cultures in Dulbecco's modified Eagle's medium. The human osteosarcoma cell line, U2OS, was obtained from the American Type Culture Collection (Manassas, VA, USA) and was grown in McCoy's 5a medium. The human osteosarcoma cell line, MNNG/HOS, was purchased from DS Pharma Biomedical (Osaka, Japan) and was maintained in Eagle's minimum essential medium containing

1% nonessential amino acids. All media were supplemented with 10% fetal bovine serum, 100 U/ml penicillin and 100 mg/ml streptomycin. The normal human lung fibroblast cell line, NHLF, was obtained from TaKaRa Biomedicals (Kyoto, Japan). NHLF cells were propagated as monolayer culture in the medium recommended by the manufacturer. Although cell lines were not authenticated by the authors, cells were immediately expanded after receipt and stored in liquid N₂. Cells were not cultured for more than 5 months following resuscitation. The cells were maintained at 37°C in a humidified atmosphere with 5% CO₂.

Recombinant adenoviruses

The recombinant telomerase-specific replication-competent adenovirus OBP-301 (Telomelysin), in which the promoter element of the *hTERT* gene drives the expression of *E1A* and *E1B* genes, was previously constructed and characterized (12, 27). For OBP-301-mediated induction of exogenous *p53* gene expression, we recently generated OBP-702, in which a human wild-type *p53* gene expression cassette was inserted into the *E3* region (Supplementary Fig. S1) (26). Ad-p53 is a replication-defective adenovirus serotype 5 vector with a *p53* gene expression cassette at the *E1* region (19, 20). Recombinant viruses were purified by ultracentrifugation

using cesium chloride step gradients, their titers were determined by a plaque-forming assay using 293 cells, and they were stored at -80°C.

Cell viability assay

Cells were seeded on 96-well plates at a density of 1×10^3 cells/well 24 h before viral infection. All cell lines were infected with OBP-702 at multiplicity of infections (MOI) of 0, 0.1, 1, 10, 50 or 100 plaque forming units (PFU)/cell. Cell viability was determined on days 1, 2, 3 and 5 after virus infection using Cell Proliferation Kit II (Roche Molecular Biochemicals, Indianapolis, IN, USA). The 50% inhibiting dose (ID₅₀) value of OBP-702 for each cell line was calculated using cell viability data obtained on day 5 after virus infection.

Time-lapse confocal laser microscopy

Green fluorescent protein (GFP)-expressing MNNG/HOS (MNNG/HOS-GFP) cells were established by stable transfection with GFP expression plasmid using Lipofectamine LTX (Invitrogen, Carlsbad, CA, USA). MNNG/HOS-GFP and NHLF cells were seeded in 35-mm glass-based dishes at a density of 1×10^5 cells/dish 24 h before infection and were infected with OBP-702 at an MOI of 10 PFU/cell for 72 h.

Phase-contrast and fluorescence time-lapse recordings were obtained to concomitantly analyze cell morphology and GFP expression using an inverted FV10i confocal laser scanning microscopy (OLYMPUS; Tokyo, Japan).

Western blot analysis

SaOS-2 and MNNG/HOS cells, seeded in a 100-mm dish at a density of 1×10^5 cells/dish, were infected with OBP-301, OBP-702 or Ad-p53 at the indicated MOIs. In contrast, SaOS-2 cells were transfected with 10 nM *miR-93* (Ambion, Austin, TX, USA), *miR-106b* (Ambion) or control miRNA (Ambion) 24 h before Ad-p53 infection and infected with Ad-p53 at an MOI of 100 for 48 h. Whole-cell lysates were prepared in a lysis buffer (50 mM Tris-HCl (pH 7.4), 150 mM NaCl, 1% Triton X-100) containing a protease inhibitor cocktail (Complete Mini; Roche, Indianapolis, IN, USA) at the indicated time points. Proteins were electrophoresed on 6% to 15% sodium dodecyl sulfate polyacrylamide gels and were transferred to polyvinylidene difluoride membranes (Hybond-P; GE Health Care, Buckinghamshire, UK). Blots were blocked with 5% non-fat dry milk in TBS-T (Tris-buffered saline and 0.1% Tween-20, pH 7.4). The primary antibodies used were: rabbit anti-PARP polyclonal antibody (pAb) (Cell Signaling Technology, Beverly, MA, USA), mouse anti-p53 monoclonal antibody

(mAb) (Calbiochem, Darmstadt, Germany), mouse anti-p21^{WAF1} mAb (Calbiochem), rabbit anti-E2F1 pAb (Santa Cruz Biotechnology, Santa Cruz, CA, USA), mouse anti-Ad5 E1A mAb (BD PharMingen, Franklin Lakes, NJ, USA), rabbit anti-microtubule-associated protein 1 light chain 3 (LC3) pAb (Medical & Biological Laboratories (MBL), Nagoya, Japan), mouse anti-p62 mAb (MBL), rabbit anti-damage-regulated autophagy modulator (DRAM) pAb (Abgent, San Diego, CA, USA), and mouse anti- β -actin mAb (Sigma-Aldrich, St. Louis, MO, USA).

Flow cytometric analysis

To analyze the active caspase-3 expression, cells were incubated for 20 min on ice in Cytofix/Cytoperm solution (BD Biosciences, Franklin Lakes, NJ, USA), were labeled with phycoerythrin-conjugated rabbit anti-active caspase-3 mAb (BD Biosciences) for 30 min, and were then analyzed using FACS array (BD Biosciences).

To evaluate the sub-G1 population, which is a apoptosis indicator, in SaOS-2 cells after virus infection, SaOS-2 cells were seeded in a 100-mm dish at a density of 1×10^6 cells/dish 24 h before viral infection, and were infected with mock, OBP-301, Ad-p53 or OBP-702 at an MOI of 10 PFUs/cell for 48 h. Cells were trypsinized and resuspended in original supernatant to ensure that both attached and non-attached cells

were analyzed. Cells stained with propidium iodide were analyzed using FACS array (BD Bioscience, Franklin Lakes, NJ, USA).

Quantitative real-time reverse transcription-PCR analysis

To evaluate the expressions of *miR-93* and *miR-106b* in tumor cells after OBP-702 infection, SaOS-2 and MNNG/HOS cells were seeded on 6-well plates at a density of 2×10^5 cells/well 24 h before viral infection and were infected with OBP-702 at MOIs of 0, 1, 5, 10, 50 or 100 PFU/cell. Three days after virus infection, total RNA was extracted from the cells using a miRNeasy Mini kit (Qiagen, Valencia, CA, USA). The concentration and quality of RNA were assessed using a Nanodrop spectrophotometer. cDNA was synthesized from 10 ng of total RNA using the TaqMan MicroRNA Reverse Transcription kit (Applied Biosystems), and quantitative real-time RT-PCR was performed using the Applied Biosystems StepOnePlus™ real-time PCR System. The expressions of *miR-93* and *miR-106b* were defined from the threshold cycle (Ct), and relative expression levels were calculated using the $2^{-\Delta\Delta Ct}$ method after normalization with reference to the expression of U6 snRNA.

***In vivo* orthotopic MNNG/HOS xenograft tumor model**

Animal experimental protocols were approved by the Ethics Review Committee for Animal Experimentation of Okayama University School of Medicine. MNNG/HOS cells (5×10^6 cells per site) were inoculated into the tibias of female athymic nude mice aged 6 to 7 weeks (CLEA Japan, Tokyo, Japan). Palpable tumors developed within 21 days and were permitted to grow to approximately 5 to 6 mm in diameter. At that stage, a 50- μ l volume of solution containing OBP-702, OBP-301 or Ad-p53 at a dose of 1×10^8 PFU or phosphate buffered saline (PBS) was injected into the tumors for three cycles every 2 days. Tumor volume was monitored by computed tomography (CT) imaging once a week after virus infection.

Three-dimensional computed tomography imaging

The tumor volume and formation of osteolytic lesions were evaluated using three-dimensional computed tomography (3D-CT) imaging (ALOKA Latheta LCT-200; Hitachi Aloka Medical, Tokyo, Japan). The tumor volume was calculated by INTAGE Realia[®] software (Cybernet Systems, Tokyo, Japan).

Histopathologic analysis

Tumors were fixed in 10% neutralized formalin and embedded in paraffin

blocks. Sections were stained with hematoxylin/eosin (H&E) and analyzed by light microscopy.

Statistical analysis

Data are expressed as means \pm SD. Student's *t* test was used to compare differences between groups. Statistical significance was defined as a *P* value less than 0.05.

Results

***In vitro* cytopathic efficacy of OBP-702 against human osteosarcoma cell lines**

To evaluate the *in vitro* cytopathic activity of OBP-702, we used the two OBP-301-sensitive human osteosarcoma cells (HOS and U2OS) and the two OBP-301-resistant human osteosarcoma cells (SaOS-2 and MNNG/HOS) that were recently described (14). The cell viability of each cell was assessed over 5 days after infection using the XTT assay. OBP-702 infection suppressed the viability of OBP-301-sensitive and OBP-301-resistant cells in dose- and time-dependent manners (Fig. 1A and 1B). When the ID₅₀ values of OBP-702 in all four human osteosarcoma

cells were compared with those of OBP-301 calculated in a previous report (14), all cell lines were more sensitive to OBP-702 than to OBP-301 (Table 1). The ID₅₀ values of OBP-702 were also lower than those of Ad-p53 (Supplementary Fig. S2). However, OBP-702 did not exhibit any cytopathic effect in NHLF cells (Fig. 1B). When GFP-expressing MNNG/HOS-GFP cells were co-cultured with human normal NHLF cells, OBP-702 infection showed a cytopathic effect (confirmed by observation of round-shaped morphological changes) in MNNG/HOS-GFP cells, but not in NHLF cells (Fig. 1C). These results indicate that OBP-702 was more cytopathic than OBP-301 for human osteosarcoma cells, but was not cytopathic for normal human cells.

Increased induction of apoptosis by OBP-702 when compared with OBP-301 or Ad-p53

We next investigated whether OBP-702 induces more profound apoptosis when compared with OBP-301 or Ad-p53. OBP-301-resistant SaOS-2 and MNNG/HOS cells were infected with OBP-702, OBP-301 or Ad-p53, and apoptosis was assessed by Western blot and flow cytometric analyzes. Western blot analysis showed that SaOS-2 cells exhibited the cleavage of PARP after infection with OBP-702 (more than 5 MOIs) or Ad-p53 (more than 50 MOIs), whereas MNNG/HOS cells had the cleavage of PARP

after infection with OBP-702 (more than 5 MOIs), but not Ad-p53 (Fig. 2A). In contrast, OBP-301 did not induce apoptosis (data not shown). Furthermore, flow cytometric analysis demonstrated that OBP-702 infection (10 MOIs) significantly increased the percentage of apoptotic cells with active caspase-3 when compared with Ad-p53 or OBP-301 at same doses in SaOS-2 and MNNG/HOS cells (Fig. 2B and 2C). Cell cycle analysis also showed that OBP-702 (10 MOIs) induced the highest percentages of sub-G1 population in SaOS-2 cells when compared with Ad-p53 or OBP-301 at same doses (Fig. 2D). These results suggest that OBP-702 induces increased apoptosis when compared with Ad-p53 or OBP-301 in human osteosarcoma cells.

p53 induction in human osteosarcoma cells infected with OBP-702

To investigate the molecular mechanism of OBP-702-induced apoptosis in human osteosarcoma cells, we evaluated p53 expression after OBP-702 infection in SaOS-2 (p53 null) and MNNG/HOS (p53 mutant) cells in which endogenous p53 expression level was confirmed by Western blot analysis (Supplementary Fig. S3). OBP-702 efficiently induced p53 expression in SaOS-2 and MNNG/HOS cells (Fig. 3A). The level of p53 expression was higher in OBP-702-treated cells than in Ad-p53-treated cells (Fig. 3A). In spite of OBP-702-induced high p53 expression,

p53-downstream target p21 protein was induced only in Ad-p53-treated cells.

To investigate the effect of exogenous p53 overexpression in virus replication, we next compared the replication abilities of OBP-702 and OBP-301 in p53-null SaOS-2 cells by measuring the relative amounts of *E1A* copy numbers. The *E1A* copy number of OBP-702 was similar to that of OBP-301 in SaOS-2 cells (Supplementary Fig. S4). These results indicate that OBP-702 efficiently induces exogenous p53 expression without affecting p21 expression and virus replication in human osteosarcoma cells.

OBP-702-mediated upregulation of *miR-93* and *miR-106b* suppresses p21 expression

Adenoviral E1A protein has been shown to activate E2F1 expression (28), which is a multifunctional transcription factor that regulates diverse cell fates through induction of many target genes, including small non-coding microRNAs (miRNAs) (29). Recently, E2F1-inducible *miR-93* and *miR-106b* have been shown to suppress p21 expression in human cancer cells (30). Therefore, we sought to investigate whether OBP-702 induces expressions of E2F1 and E2F1-regulated miRNAs (*miR-93* and *miR-106b*). OBP-702 infection activated E2F1 expression along with E1A accumulation

in SaOS-2 and MNNG/HOS cells (Fig. 3B). The expression levels of *miR-93* and *miR-106b* were increased in association with E2F1 activation in OBP-702-infected SaOS-2 and MNNG/HOS cells (Fig. 3C). In contrast, E1A-deleted Ad-p53 infection did not increase expressions of E2F1 and E2F1-regulated *miR-93* and *miR-106b* (data not shown). Next, we assessed whether upregulation of *miR-93* and *miR-106b* efficiently suppresses p21 expression induced by Ad-p53-mediated p53 overexpression. Ad-p53 infection at MOIs of 10 and 100 efficiently induced p21 expression at 48 h after infection in SaOS-2 cells (Supplementary Fig. S5). When SaOS-2 cells were infected with Ad-p53 at an MOI of 100 for 48 h, pre-transfection with *miR-93*, *miR-106b* or both efficiently suppressed Ad-p53-induced p21 expression (Fig. 3D). Interestingly, both *miR-93* and *miR-106b* -transfected SaOS-2 cells showed the 1.5-fold increased expression of cleaved PARP (C-PARP) in consistent with remarkable p21 downregulation when compared with those transfected with control miR. However, the expression level of C-PARP was not increased in the *miR-93* or *miR-106b*-transfected SaOS-2 cells, although transfection with *miR-93* or *miR-106b* moderately decreased p21 expression. These results suggest that OBP-702 suppresses p21 expression through E1A-dependent upregulation of E2F1-inducible both *miR-93* and *miR-106b* and contributes to induction of apoptosis.

Increased induction of autophagy by OBP-702 when compared with OBP-301

Recently, we demonstrated that oncolytic adenovirus OBP-301 mainly induces programmed cell death in association with autophagy rather than apoptosis in human tumor cells (31). Therefore, we next investigated whether OBP-702 induces more profound autophagy than does OBP-301. Western blot analysis revealed that OBP-702 infection showed increased autophagy, which was confirmed by conversion of LC3-I to LC3-II (increased ratio of LC3-II/LC3-I) and p62 downregulation, when compared with OBP-301 in MNNG/HOS cells (Fig. 4A). Moreover, the expression level of the p53-induced modulator of autophagy, DRAM (32), was decreased after OBP-301 infection, but its expression was maintained after OBP-702 infection (Fig. 4A). Since p53-mediated p21 overexpression is known to inhibit both apoptosis and autophagy (17, 18), we further evaluated whether miR-mediated p21 suppression is involved in the enhancement of p53-mediated autophagy induction. Ad-p53-induced autophagy was enhanced by *miR-93* and *miR-106b* -mediated p21 suppression (Fig. 4B). These results suggest that OBP-702 induces more profound autophagy than does OBP-301 and that this effect occurs via p53-mediated DRAM activation and miR-mediated p21 suppression.

Enhanced antitumor effect of OBP-702 in an orthotopic xenograft tumor model

Finally, to assess the *in vivo* antitumor effect of OBP-702, we used an orthotopic MNNG/HOS tumor xenograft model. OBP-702, OBP-301, Ad-p53 or PBS was intratumorally injected for three cycles every 2 days. OBP-702 administration significantly suppressed tumor growth when compared with OBP-301, Ad-p53 or PBS in an orthotopic MNNG/HOS tumor model (Fig. 5A and B). 3D-CT examination revealed that OBP-702-treated tumors had less bone destruction than did OBP-301- or Ad-p53-treated tumors (Fig. 5C). On histopathologic analysis, there were large necrotic areas in OBP-702-treated tumors, but not in OBP-301- or Ad-p53-treated tumors (Fig. 5D). Moreover, the expression of the cell proliferation marker, Ki67, was also decreased, especially in OBP-702-treated tumor cells (Supplementary Fig. S6). These results suggest that OBP-702 eliminates tumor tissues more efficiently when compared with OBP-301 or Ad-p53.

Discussion

We previously reported that telomerase-specific replication-competent

oncolytic adenovirus OBP-301 has strong antitumor activity in a variety of human epithelial and non-epithelial malignant cells (12, 14, 27). However, some human osteosarcoma cells were resistant to the cytopathic activity of OBP-301 (14). In this study, we demonstrated that a novel p53-expressing oncolytic adenovirus, OBP-702, had increased *in vitro* and *in vivo* antitumor effects than did OBP-301 in human osteosarcoma cells (Fig. 1 and 5). OBP-702 induced increased apoptosis in association with p53 upregulation and p21 downregulation when compared with replication-deficient Ad-p53 (Fig. 2 and 3A). E1A-dependent upregulation of *miR-93* and *miR-106b* was involved in OBP-702-mediated suppression of p21 expression (Fig. 3). Moreover, p53-mediated DRAM activation with p21 suppression enhanced oncolytic adenovirus-mediated autophagy induction (Fig. 4). Recent studies suggest that transgene-expressing armed oncolytic adenoviruses are a promising antitumor strategy for induction of oncolytic and transgene-induced cell death (33). Although p53 overexpression has been shown to enhance antitumor activity of oncolytic adenoviruses (34), the molecular mechanisms by which p53 mediates enhancement of the antitumor effect remain unclear. Recently, we reported that OBP-702 induces profound apoptosis through p53-dependent BAX upregulation and E1A-dependent p21 and MDM2 downregulation in epithelial malignant cells (26). Thus, oncolytic adenovirus-mediated

p53 overexpression likely induces dual apoptotic and autophagic cell death pathways through p53-dependent BAX/DRAM activation and E1A-dependent p21/MDM2 suppression with E2F1-inducible *miR-93/106b* upregulation (Fig. 6).

OBP-702 efficiently suppressed the cell viability of both OBP-301-sensitive and OBP-301-resistant osteosarcoma cells (Fig. 1). We previously reported that OBP-301-resistant SaOS-2 cells have no *hTERT* mRNA expression (Table 1), suggesting that SaOS-2 cells maintain telomere length through alternative lengthening of telomeres (ALT). As *hTERT* gene promoter is used for tumor-specific replication of OBP-301, ALT-type human osteosarcoma cells like SaOS-2 cells may be resistant to OBP-301. However, ALT-type SaOS-2 cells showed similar sensitivity to OBP-702 as well as non-ALT-type MNNG/HOS cells (Fig. 1 and Table 1). These results suggest that p53 overexpression overcomes resistance to OBP-301 in ALT-type SaOS-2 cells. Since the replication rate of OBP-702 was almost similar that of OBP-301 in ALT-type SaOS-2 cells (Supplementary Fig. S2), p53-induced cell death pathway would suppress the cell viability of ALT-type human osteosarcoma cells.

OBP-702-mediated p53 overexpression induced two types of programmed cell deaths (i.e., apoptosis and autophagy), thereby contributing to the enhancement of the antitumor effect of OBP-301 in human osteosarcoma cells (Fig. 2 and 4). Since

p53-downstream target p21 functions as a suppressor of apoptosis and autophagy (17, 18), p21 suppression may be a critical factor to induce dual programmed cell death pathways in response p53 overexpression. Suppression of p21 expression by genetic deletion or artificial p21-target microRNA has been shown to enhance the Ad-p53-induced apoptosis (18, 35). Inactivation of p21 by adenoviral E1A has been shown to enhance apoptosis in chemotherapeutic drug-treated human colon cancer cells that overexpress p53 (36). Genetic deletion of p21 has been also shown to induce autophagy in mouse embryonic fibroblasts treated with C(2)-ceramide or gamma-irradiation (17). In contrast, p21 overexpression inhibited the Ad-p53-mediated apoptosis induction (18). Thus, E1A-mediated p21 downregulation would enhance p53-induced apoptosis and autophagy in OBP-702-infected cells.

E1A-dependent E2F1 activation and subsequent upregulation of E2F1-inducible miRNAs efficiently suppressed p21 expression, leading to the enhancement of p53-induced apoptosis and autophagy, in OBP-702-infected osteosarcoma cells (Fig. 2, 3 and 4). Recent studies suggest that the cross-talk between p53 and E2F1 play a role in the regulation of diverse cell fates (37). For example, co-expression of p53 and E2F1 contributes to induction of apoptosis (38, 39). We previously demonstrated that E2F1 enhanced Ad-p53-mediated apoptosis through

p14ARF-dependent MDM2 downregulation (39) and that OBP-702 infection showed E1A-dependent MDM2 downregulation in association with apoptosis (26). Recently, E2F1 has been shown to suppress MDM2 expression by suppressing the promoter activity (40) or by inducing upregulation of *miR-25/32*, which targets MDM2 (41). Furthermore, E2F1-inducible *miR-93/106b* enhanced Ad-p53-induced apoptosis and autophagy via p21 suppression (Fig. 3D and 4B). Therefore, the cooperation between the MDM2-p53-p21 pathway and the E2F1-miRNA pathway may be involved in the induction of apoptotic and autophagic cell death in response to OBP-702.

OBP-702-mediated p53 overexpression enhanced autophagy that was induced by oncolytic adenovirus in human osteosarcoma cells. OBP-702 infection induced increased expression of DRAM and decreased expression of p62 when compared with OBP-301 (Fig. 4), suggesting that OBP-702-mediated p53 overexpression enhances autophagy through DRAM activation. We recently reported that OBP-301 induces autophagy through E1A-dependent activation of E2F1-*miR-7* pathway and subsequent suppression of epidermal growth factor receptor (EGFR) (31). Restoration of p53 expression enhances the sensitivity to EGFR inhibitors in human cancer cells (42). Moreover, EGFR downregulation by transfection of specific antisense oligonucleotide promotes the differentiation status of human osteosarcoma U2OS cells (43). Thus,

OBP-702 may induce differentiation as well as cell death through autophagy activation by DRAM upregulation and EGFR downregulation in human osteosarcoma cells.

The 3D-CT imaging system was a useful method to assess both tumor volume and bone destruction status in MNNG/HOS tumors. OBP-702-treated tumors were smaller and had less bone destruction when compared with PBS-, Ad-p53- or OBP-301-treated tumors (Fig. 5A and 5C). Recent reports have suggested that zoledronic acid suppresses tumor growth as well as osteolytic components in human osteosarcoma xenograft tumor models (44, 45). These results suggest that combination therapy with OBP-702 and zoledronic acid may be more effective and more protective against bone destruction in human osteosarcomas. Further study using a 3D-CT imaging system may provide important information regarding bone destruction status in osteosarcomas treated with OBP-702 and zoledronic acid.

Adenovirus-mediated p53 gene therapy exerts an antitumor effect in human osteosarcoma cells (46). However, the antitumor activity of replication-deficient Ad-p53 is limited in some human osteosarcoma cells (47). Ad-p53-mediated p53 overexpression increases the sensitivity of human osteosarcoma cells to the chemotherapeutic drugs, cisplatin and doxorubicin (48). A synergistic antitumor effect between doxorubicin and roscovitine was also associated with autophagy induction in human osteosarcoma U2OS

cells (49). As OBP-702 induced more profound apoptosis and autophagy than did OBP-301 or Ad-p53 (Fig. 2 and 4), combination therapy with OBP-702 and chemotherapeutic agents may be more effective than monotherapy with OBP-702. Moreover, a recent report has shown that p53-armed replication-competent oncolytic adenovirus is a safe antitumor agent in rodents and nonhuman primates (50). However, for clinical application of OBP-702, it must be necessary to establish the systemic delivery method and confirm the host biological contributions in cancer patients. Although there are some unsolved issues, the combination of p53-armed oncolytic adenovirus and chemotherapy may provide us a promising antitumor strategy against human osteosarcoma cells.

In conclusion, we clearly demonstrated that the p53-expressing oncolytic adenovirus OBP-702 has a much stronger antitumor effect than does OBP-301. Oncolytic adenovirus-mediated p53 gene transduction may induce dual apoptotic and autophagic cell death pathways through p53-dependent activation of cell death inducers and E1A-dependent suppression of cell death inhibitors, resulting in the enhancement of antitumor effect.

Acknowledgements

We thank Dr. Satoru Kyo (Kanazawa University) for providing the HOS and SaOS-2 cells. We also thank Ms. Tomoko Sueishi for her excellent technical support.

References

1. Ottaviani G, Jaffe N. The etiology of osteosarcoma. *Cancer Treat Res.* 2009;152:15-32.
2. Damron TA, Ward WG, Stewart A. Osteosarcoma, chondrosarcoma, and Ewing's sarcoma: National Cancer Data Base Report. *Clin Orthop Relat Res.* 2007;459:40-7.
3. Lewis IJ, Nooij MA, Whelan J, Sydes MR, Grimer R, Hogendoorn PC, et al. Improvement in histologic response but not survival in osteosarcoma patients treated with intensified chemotherapy: a randomized phase III trial of the European Osteosarcoma Intergroup. *J Natl Cancer Inst.* 2007;99:112-28.
4. Bacci G, Longhi A, Versari M, Mercuri M, Briccoli A, Picci P. Prognostic factors for osteosarcoma of the extremity treated with neoadjuvant chemotherapy: 15-year experience in 789 patients treated at a single institution. *Cancer.* 2006;106:1154-61.
5. Bielack SS, Kempf-Bielack B, Delling G, Exner GU, Flege S, Helmke K, et al. Prognostic factors in high-grade osteosarcoma of the extremities or trunk: an analysis of 1,702 patients treated on neoadjuvant cooperative osteosarcoma study group protocols. *J Clin Oncol.* 2002;20:776-90.
6. Siegel R, Naishadham D, Jemal A. Cancer statistics, 2012. *CA Cancer J Clin.* 2012;62:10-29.
7. Buseman CM, Wright WE, Shay JW. Is telomerase a viable target in cancer? *Mutat Res.* 2012;730:90-7.
8. Artandi SE, DePinho RA. Telomeres and telomerase in cancer. *Carcinogenesis.* 2010;31:9-18.
9. Umehara N, Ozaki T, Sugihara S, Kunisada T, Morimoto Y, Kawai A, et al. Influence of telomerase activity on bone and soft tissue tumors. *J Cancer Res Clin Oncol.* 2004;130:411-6.
10. Aogi K, Woodman A, Urquidi V, Mangham DC, Tarin D, Goodison S. Telomerase activity in soft-tissue and bone sarcomas. *Clin Cancer Res.* 2000;6:4776-81.
11. Nakayama J, Tahara H, Tahara E, Saito M, Ito K, Nakamura H, et al. Telomerase activation by hTERT in human normal fibroblasts and hepatocellular carcinomas. *Nat Genet.* 1998;18:65-8.
12. Kawashima T, Kagawa S, Kobayashi N, Shirakiya Y, Umeoka T, Teraishi F, et al. Telomerase-specific replication-selective virotherapy for human cancer. *Clin*

- Cancer Res. 2004;10:285-92.
13. Nemunaitis J, Tong AW, Nemunaitis M, Senzer N, Phadke AP, Bedell C, et al. A phase I study of telomerase-specific replication competent oncolytic adenovirus (telomelysin) for various solid tumors. *Mol Ther*. 2010;18:429-34.
 14. Sasaki T, Tazawa H, Hasei J, Kunisada T, Yoshida A, Hashimoto Y, et al. Preclinical evaluation of telomerase-specific oncolytic virotherapy for human bone and soft tissue sarcomas. *Clin Cancer Res*. 2011;17:1828-38.
 15. Li G, Kawashima H, Ogose A, Ariizumi T, Xu Y, Hotta T, et al. Efficient virotherapy for osteosarcoma by telomerase-specific oncolytic adenovirus. *J Cancer Res Clin Oncol*. 2011;137:1037-51.
 16. Vousden KH, Prives C. Blinded by the Light: The Growing Complexity of p53. *Cell*. 2009;137:413-31.
 17. Fujiwara K, Daido S, Yamamoto A, Kobayashi R, Yokoyama T, Aoki H, et al. Pivotal role of the cyclin-dependent kinase inhibitor p21WAF1/CIP1 in apoptosis and autophagy. *J Biol Chem*. 2008;283:388-97.
 18. Gorospe M, Cirielli C, Wang X, Seth P, Capogrossi MC, Holbrook NJ. p21(Waf1/Cip1) protects against p53-mediated apoptosis of human melanoma cells. *Oncogene*. 1997;14:929-35.
 19. Blagosklonny MV, el-Deiry WS. In vitro evaluation of a p53-expressing adenovirus as an anti-cancer drug. *Int J Cancer*. 1996;67:386-92.
 20. Zeng Y, Prabhu N, Meng R, Eldeiry W. Adenovirus-mediated p53 gene therapy in nasopharyngeal cancer. *Int J Oncol*. 1997;11:221-6.
 21. Clayman GL, el-Naggar AK, Lippman SM, Henderson YC, Frederick M, Merritt JA, et al. Adenovirus-mediated p53 gene transfer in patients with advanced recurrent head and neck squamous cell carcinoma. *J Clin Oncol*. 1998;16:2221-32.
 22. Swisher SG, Roth JA, Nemunaitis J, Lawrence DD, Kemp BL, Carrasco CH, et al. Adenovirus-mediated p53 gene transfer in advanced non-small-cell lung cancer. *J Natl Cancer Inst*. 1999;91:763-71.
 23. Shimada H, Matsubara H, Shiratori T, Shimizu T, Miyazaki S, Okazumi S, et al. Phase I/II adenoviral p53 gene therapy for chemoradiation resistant advanced esophageal squamous cell carcinoma. *Cancer Sci*. 2006;97:554-61.
 24. Fujiwara T, Tanaka N, Kanazawa S, Ohtani S, Saijo Y, Nukiwa T, et al. Multicenter phase I study of repeated intratumoral delivery of adenoviral p53 in patients with advanced non-small-cell lung cancer. *J Clin Oncol*. 2006;24:1689-99.
 25. Sakai R, Kagawa S, Yamasaki Y, Kojima T, Uno F, Hashimoto Y, et al. Preclinical evaluation of differentially targeting dual virotherapy for human solid cancer. *Mol*

- Cancer Ther. 2010;9:1884-93.
26. Yamasaki Y, Tazawa H, Hashimoto Y, Kojima T, Kuroda S, Yano S, et al. A novel apoptotic mechanism of genetically engineered adenovirus-mediated tumour-specific p53 overexpression through E1A-dependent p21 and MDM2 suppression. *Eur J Cancer*. 2012;48:2282-91.
 27. Hashimoto Y, Watanabe Y, Shirakiya Y, Uno F, Kagawa S, Kawamura H, et al. Establishment of biological and pharmacokinetic assays of telomerase-specific replication-selective adenovirus. *Cancer Sci*. 2008;99:385-90.
 28. Bagchi S, Raychaudhuri P, Nevins JR. Adenovirus E1A proteins can dissociate heteromeric complexes involving the E2F transcription factor: a novel mechanism for E1A trans-activation. *Cell*. 1990;62:659-69.
 29. Emmrich S, Putzer BM. Checks and balances: E2F-microRNA crosstalk in cancer control. *Cell Cycle*. 2010;9:2555-67.
 30. Petrocca F, Vecchione A, Croce CM. Emerging role of miR-106b-25/miR-17-92 clusters in the control of transforming growth factor beta signaling. *Cancer research*. 2008;68:8191-4.
 31. Tazawa H, Yano S, Yoshida R, Yamasaki Y, Sasaki T, Hashimoto Y, et al. Genetically engineered oncolytic adenovirus induces autophagic cell death through an E2F1-microRNA-7-epidermal growth factor receptor axis. *Int J Cancer*. 2012;131:2939-50.
 32. Crighton D, Wilkinson S, O'Prey J, Syed N, Smith P, Harrison PR, et al. DRAM, a p53-induced modulator of autophagy, is critical for apoptosis. *Cell*. 2006;126:121-34.
 33. Liu TC, Galanis E, Kim D. Clinical trial results with oncolytic virotherapy: a century of promise, a decade of progress. *Nat Clin Pract Oncol*. 2007;4:101-17.
 34. van Beusechem VW, van den Doel PB, Grill J, Pinedo HM, Gerritsen WR. Conditionally replicative adenovirus expressing p53 exhibits enhanced oncolytic potency. *Cancer Res*. 2002;62:6165-71.
 35. Idogawa M, Sasaki Y, Suzuki H, Mita H, Imai K, Shinomura Y, et al. A single recombinant adenovirus expressing p53 and p21-targeting artificial microRNAs efficiently induces apoptosis in human cancer cells. *Clin Cancer Res*. 2009;15:3725-32.
 36. Chattopadhyay D, Ghosh MK, Mal A, Harter ML. Inactivation of p21 by E1A leads to the induction of apoptosis in DNA-damaged cells. *J Virol*. 2001;75:9844-56.
 37. Polager S, Ginsberg D. p53 and E2f: partners in life and death. *Nat Rev Cancer*. 2009;9:738-48.

38. Wu X, Levine AJ. p53 and E2F-1 cooperate to mediate apoptosis. *Proc Natl Acad Sci U S A*. 1994;91:3602-6.
39. Itoshima T, Fujiwara T, Waku T, Shao J, Kataoka M, Yarbrough WG, et al. Induction of apoptosis in human esophageal cancer cells by sequential transfer of the wild-type p53 and E2F-1 genes: involvement of p53 accumulation via ARF-mediated MDM2 down-regulation. *Clin Cancer Res*. 2000;6:2851-9.
40. Tian X, Chen Y, Hu W, Wu M. E2F1 inhibits MDM2 expression in a p53-dependent manner. *Cell Signal*. 2011;23:193-200.
41. Suh SS, Yoo JY, Nuovo GJ, Jeon YJ, Kim S, Lee TJ, et al. MicroRNAs/TP53 feedback circuitry in glioblastoma multiforme. *Proc Natl Acad Sci U S A*. 2012;109:5316-21.
42. Huang S, Benavente S, Armstrong EA, Li C, Wheeler DL, Harari PM. p53 modulates acquired resistance to EGFR inhibitors and radiation. *Cancer Res*. 2011;71:7071-9.
43. Salvatori L, Caporuscio F, Coroniti G, Starace G, Frati L, Russo MA, et al. Down-regulation of epidermal growth factor receptor induced by estrogens and phytoestrogens promotes the differentiation of U2OS human osteosarcoma cells. *J Cell Physiol*. 2009;220:35-44.
44. Dass CR, Choong PF. Zoledronic acid inhibits osteosarcoma growth in an orthotopic model. *Mol Cancer Ther*. 2007;6:3263-70.
45. Labrinidis A, Hay S, Liapis V, Ponomarev V, Findlay DM, Evdokiou A. Zoledronic acid inhibits both the osteolytic and osteoblastic components of osteosarcoma lesions in a mouse model. *Clin Cancer Res*. 2009;15:3451-61.
46. Ternovoi VV, Curiel DT, Smith BF, Siegal GP. Adenovirus-mediated p53 tumor suppressor gene therapy of osteosarcoma. *Lab Invest*. 2006;86:748-66.
47. Hellwinkel OJ, Muller J, Pollmann A, Kabisch H. Osteosarcoma cell lines display variable individual reactions on wildtype p53 and Rb tumour-suppressor transgenes. *J Gene Med*. 2005;7:407-19.
48. Ganjavi H, Gee M, Narendran A, Parkinson N, Krishnamoorthy M, Freedman MH, et al. Adenovirus-mediated p53 gene therapy in osteosarcoma cell lines: sensitization to cisplatin and doxorubicin. *Cancer Gene Ther*. 2006;13:415-9.
49. Lambert LA, Qiao N, Hunt KK, Lambert DH, Mills GB, Meijer L, et al. Autophagy: a novel mechanism of synergistic cytotoxicity between doxorubicin and roscovitine in a sarcoma model. *Cancer Res*. 2008;68:7966-74.
50. Su C, Cao H, Tan S, Huang Y, Jia X, Jiang L, et al. Toxicology profiles of a novel p53-armed replication-competent oncolytic adenovirus in rodents, felids, and

nonhuman primates. *Toxicol Sci.* 2008;106:242-50.

Table 1. Comparison of ID₅₀ values of OBP-301 and OBP-702 in various human osteosarcoma cell lines

Cell lines	Sensitivity to OBP-301	Cell type*	Relative hTERT mRNA expression	ID ₅₀ value** (MOI)		Ratio† (OBP-702/OBP-301)
				OBP-301	OBP-702	
SaOS-2	Resistant	ALT	negative	98.1	5.5	0.06
MNNG/HOS	Resistant	non-ALT	1	97.3	6.7	0.07
U2OS	Sensitive	ALT	0.3	38.2	1.2	0.03
HOS	Sensitive	non-ALT	4.3	43.0	4.5	0.10

* Alternative lengthening of telomeres (ALT).

** The ID₅₀ values of OBP-702 and OBP-301 were calculated from the data of XTT assay on day 5 after infection.

† The ratio was calculated from the division of the ID₅₀ value of OBP-702 by the ID₅₀ value of OBP-301.

Figure legends

Fig. 1. *In vitro* cytopathic effect of OBP-702 in human osteosarcoma cell lines. A, OBP-301-sensitive (HOS and U2OS) and OBP-301-resistant (SaOS-2 and MNNG/HOS) human osteosarcoma cells were infected with OBP-702 at the indicated multiplicity of infection (MOI), and cell viability was quantified over 5 days using the XTT assay. Cell viability was calculated relative to that of the mock-infected group on each day, which was set at 1.0. Cell viability data are expressed as mean values \pm SD (n = 5). B, four human osteosarcoma cells and one normal fibroblast NHLF cells were seeded 24 h before viral infection, and were infected with OBP-702 at the indicated MOIs, and cell viability was examined on day 5 using the XTT assay. Cell viability was calculated relative to that of the mock-infected group, which was set at 1.0. Cell viability data are expressed as mean \pm SD (n = 5). C, time-lapse images of cytopathic effect of OBP-702 in co-culture of green fluorescent protein (GFP)-expressing MNNG/HOS cells with human normal fibroblast NHLF cells. MNNG/HOS-GFP cells co-incubated with NHLF cells were recorded for 72 h after OBP-702 infection at an MOI of 10. Three images on the left are low-magnification, and one image on the right is high-magnification of the area outlined by a white square. Left scale bars, 100 μ m.

Right scale bar, 10 μ m.

Fig. 2. OBP-702 induces increased apoptosis when compared with OBP-301 or

Ad-p53. **A**, OBP-301-resistant SaOS-2 and MNNG/HOS cells were infected with OBP-702 or Ad-p53 at the indicated MOIs for 72 h. Cell lysates were subjected to Western blot analysis for the cleaved PARP (C-PARP) and PARP. β -actin was assayed as a loading control. **B-D**, SaOS-2 and MNNG/HOS cells were infected with OBP-702, OBP-301 or Ad-p53 at an MOI of 10 for 48 h. Mock-infected cells were used as control. Caspase-3 activation was quantified using the flow cytometric analysis. Representative flow cytometric data were shown (**B**). The mean percentage of SaOS-2 cells and MNNG/HOS cells that express active caspase-3 was calculated based on three-independent experiments (**C**). The cell cycle state was analyzed by flow cytometry in SaOS-2 cells after staining with propidium iodide. Representative cell cycle data were shown (**D**). The percentage of sub-G1 population was expressed in each graph. Bars, SD. Statistical significance was determined using Student's *t* test. *, $P < 0.05$.

Fig. 3. OBP-702 induces p53 overexpression with E1A-mediated p21 suppression

via *miR-93* and *miR-106b* activation. **A**, expression of the p53 and p21 proteins in

SaOS-2 and MNNG/HOS cells infected with OBP-702 or Ad-p53 at the indicated MOIs for 72 h was assessed using Western blot analysis. **B**, expression of the E2F1 and viral E1A proteins in SaOS-2 and MNNG/HOS cells infected with OBP-702 at the indicated MOIs for 72 h was assessed using Western blot analysis. **C**, expression of *miR-93* and *miR-106b* was assayed using qRT-PCR in SaOS-2 cells infected with OBP-702 at the indicated MOIs for 72 h on three-independent experiments. The values of *miR-93* and *miR-106b* at 0 MOI were set at 1, and the relative levels of *miR-93* and *miR-106b* at the indicated MOIs were plotted as fold induction. Bars, SD. Statistical significance was determined by Student's *t* test. *, $P < 0.05$. **D**, SaOS-2 cells were transfected with 10 nM *miR-93*, *miR-106* or control miRNA 24 h before Ad-p53 infection at an MOI of 100. At 48 h after Ad-p53 infection, the expression levels of p53, p21, PARP and cleaved PARP (C-PARP) were examined by Western blot analysis. β -actin was assayed as a loading control. By using ImageJ software, the expression level of C-PARP protein was calculated relative to its expression in the control miR-treated cells, whose expression level was designated as 1.0.

Fig. 4. OBP-702 induces increased autophagy when compared with OBP-301. A, MNNG/HOS cells were infected with OBP-702 or OBP-301 at the indicated MOIs for

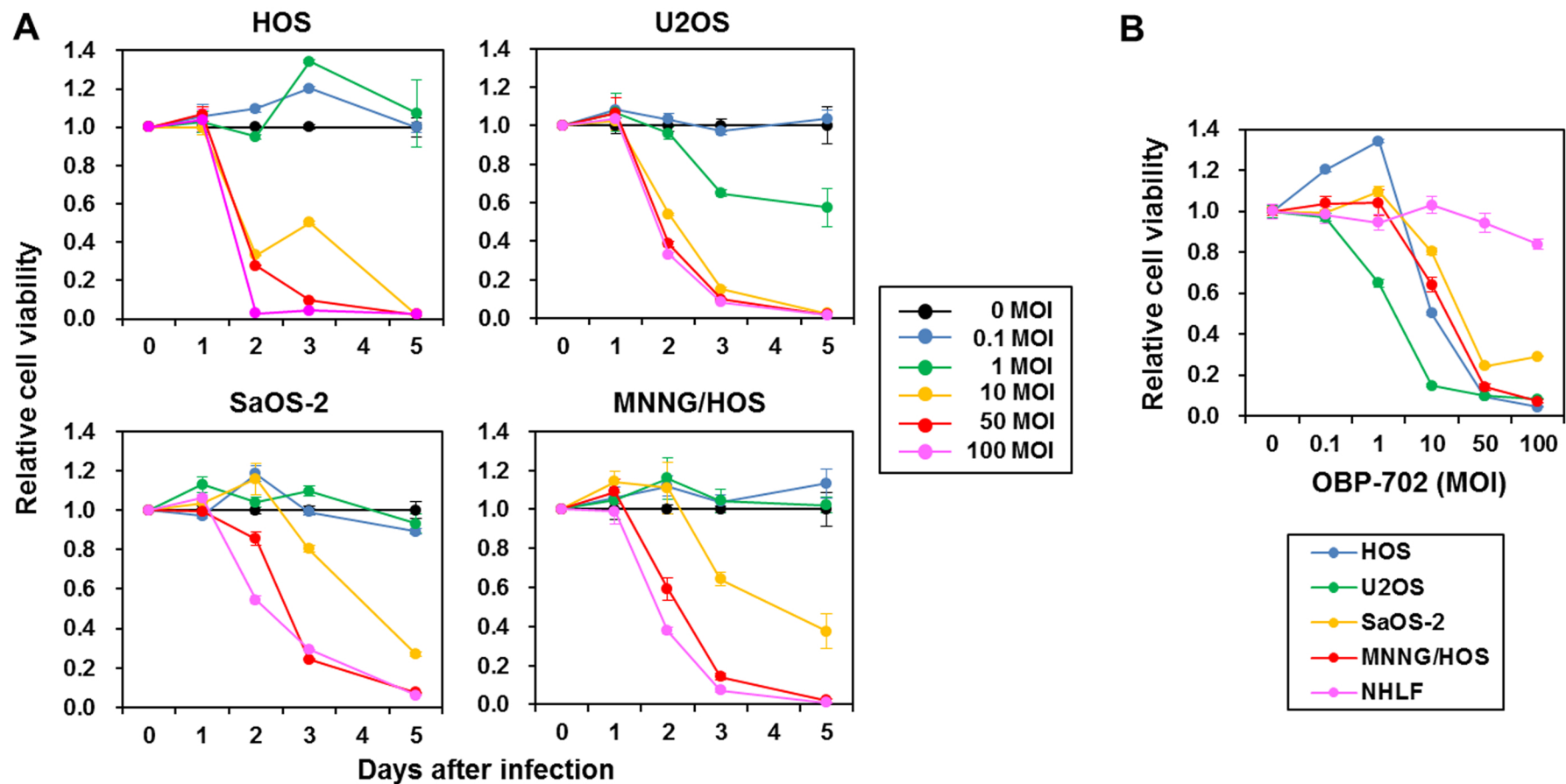
72 h. Cell lysates were subjected to Western blot analysis for LC3, p62 and DRAM. **B**, SaOS-2 cells were transfected with 10 nM *miR-93*, *miR-106* or control miRNA 24 h before Ad-p53 infection. At 48 h after Ad-p53 infection at an MOI of 100, the expression levels of LC3, p62 and DRAM were examined by Western blot analysis. β -actin was assayed as a loading control. By using ImageJ software, the ratio of LC3-II/LC3-I expressions was calculated relative to its expression in the mock-infected cells, whose expression level was designated as 1.0.

Fig. 5. Antitumor effect of OBP-702 in an orthotopic MNNG/HOS osteosarcoma

xenograft model. **A**, athymic nude mice were inoculated intratibially with MNNG/HOS cells (5×10^6 cells/site). Twenty-one days after inoculation (designated as day 0), Ad-p53, OBP-301 or OBP-702 was injected into the tumor with 1×10^8 PFUs on days 0, 2 and 4 (black arrows). PBS was used as a control. Three mice were used for each group. Each tumor volume was assessed by computed tomography (CT) examination. Tumor growth was expressed as mean tumor volume \pm SD. Statistical significance was determined by Student's *t* test. *, $P < 0.05$. **B**, macroscopic appearance of MNNG/HOS tumors in nude mice on days 0 and 28 after treatment with PBS, Ad-p53, OBP-301 or OBP-702. Tumor masses are outlined by a dotted line. **C**,

three-dimensional (3D)-CT images of MNNG/HOS tumors. The tumor volumes were calculated by the image viewer (INTAGE Realia) based on 3D-CT images of tumors after trimming. The white arrowheads indicate the osteolytic areas within tumor tissues treated with PBS, Ad-p53 or OBP-301. Left side images are low-magnification, and right side images are high-magnification of the area outlined by a white square. **D**, histological analysis of the MNNG/HOS tumors. Tumor tissues were obtained on day 28 after first treatment with PBS, Ad-p53, OBP-301 or OBP-702. Paraffin-embedded sections of MNNG/HOS tumors were stained with hematoxylin and eosin solutions. There were large necrotic areas in MNNG/HOS tumors treated with OBP-702. Left side images are low-magnification, and right side images are high-magnification of the area outlined by a white square. Left scale bars, 500 μm . Right scale bars, 100 μm .

Fig. 6. Outline of OBP-702-mediated induction of dual programmed cell death pathways. OBP-702 infection induces apoptosis and autophagy, leading to cell death, through p53-dependent BAX/DRAM upregulation and E1A-dependent p21 downregulation via E2F1-inducible *miR-93/106b* activation.



C

Co-culture of MNNG/HOS-GFP and NHLF cells

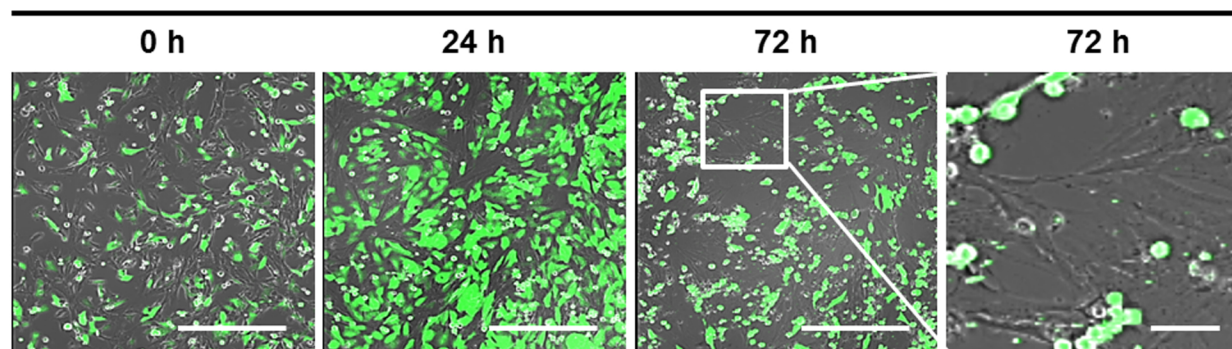


Fig. 1

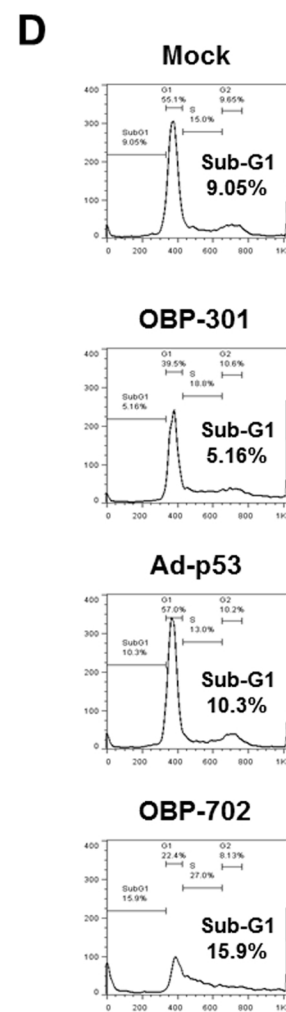
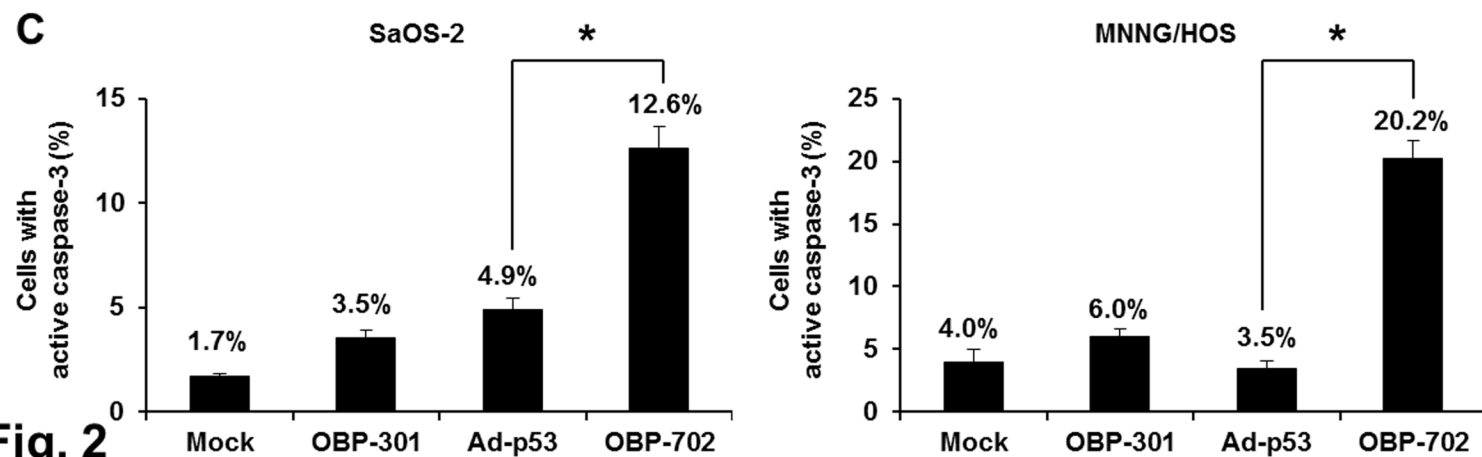
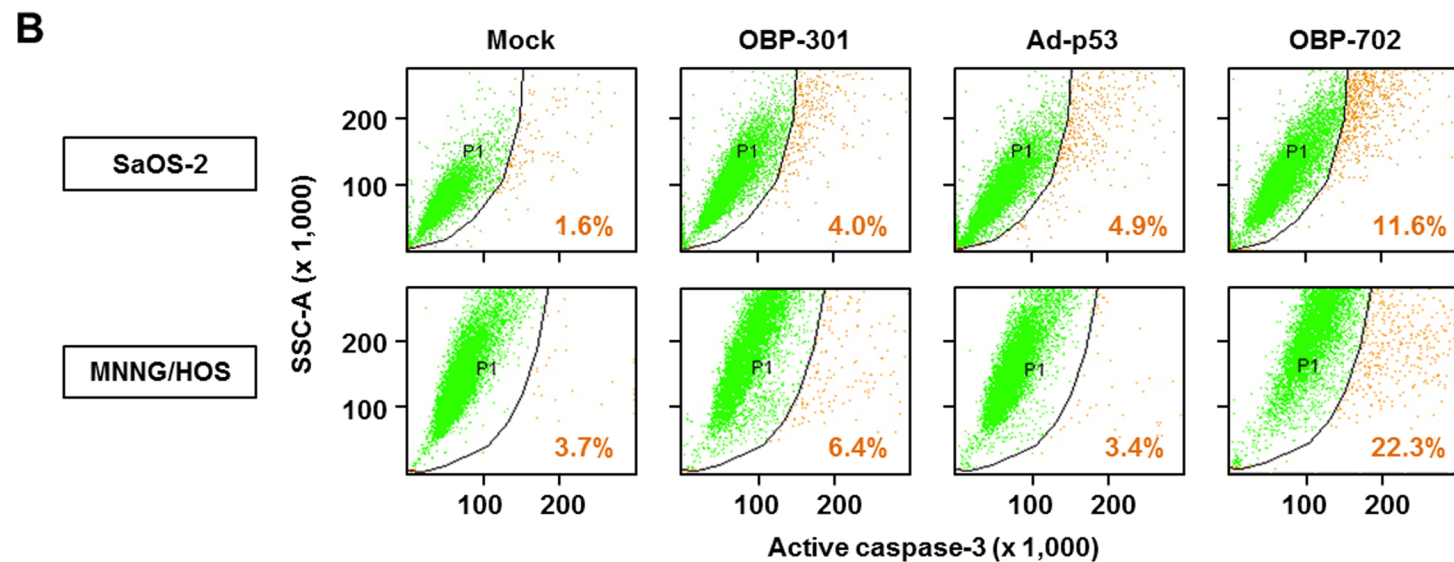
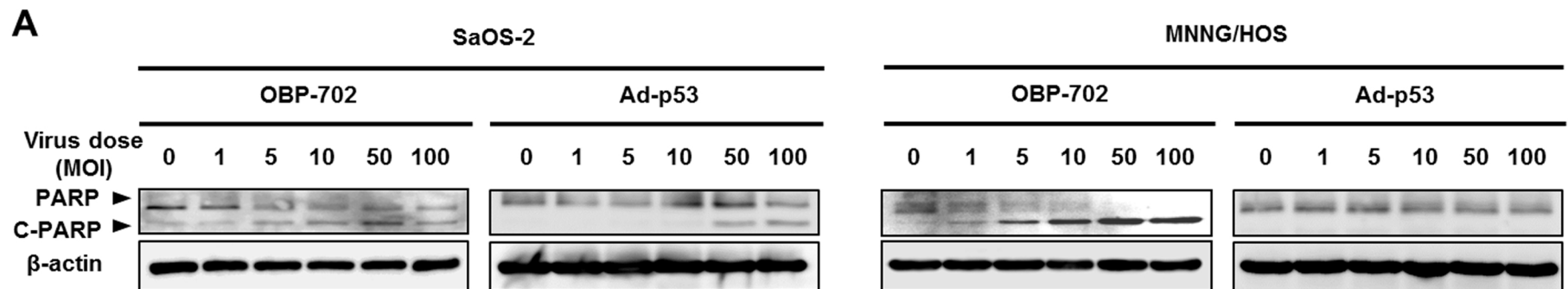


Fig. 2

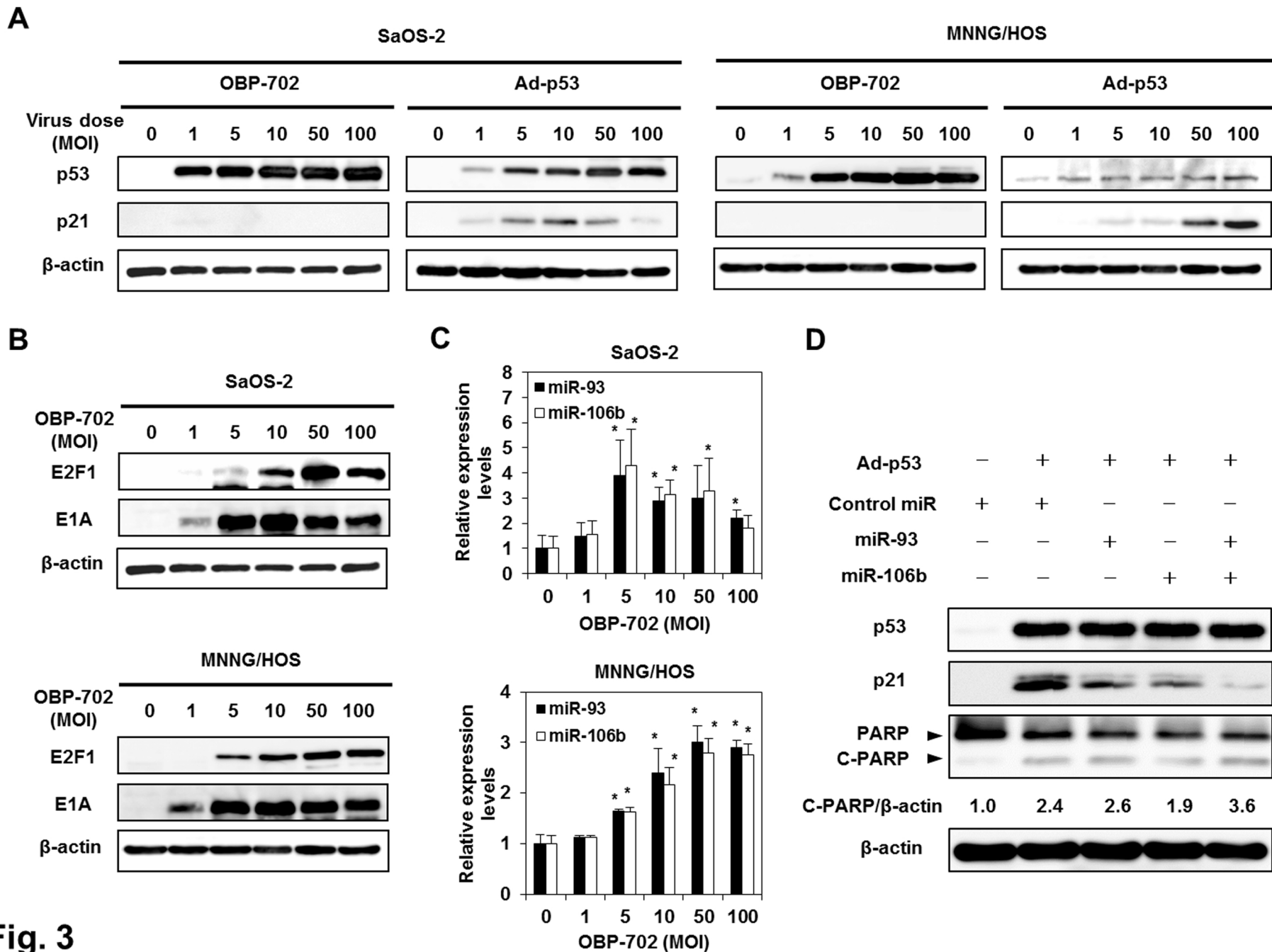


Fig. 3

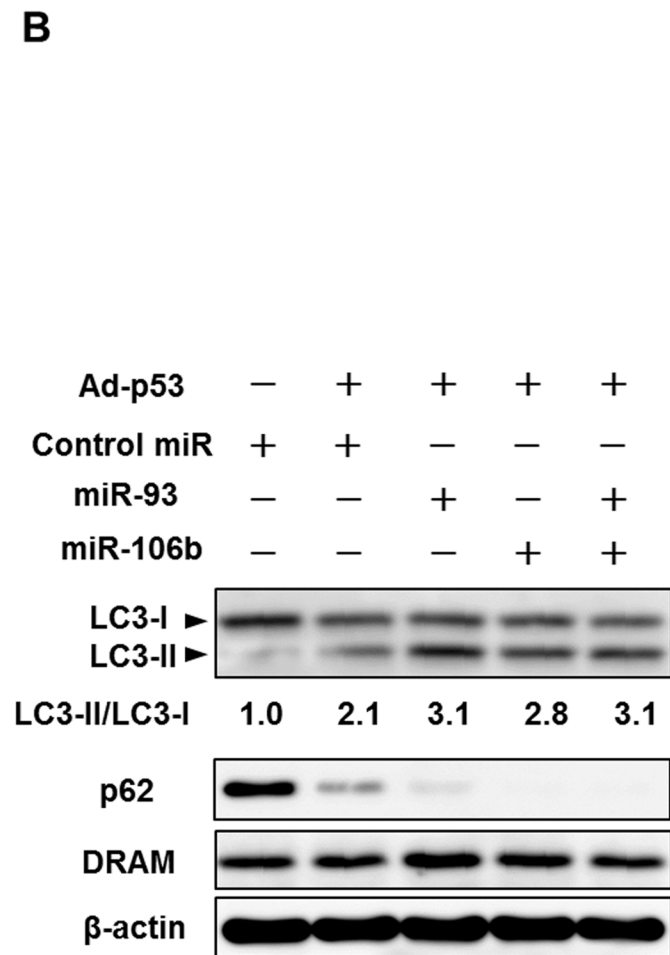
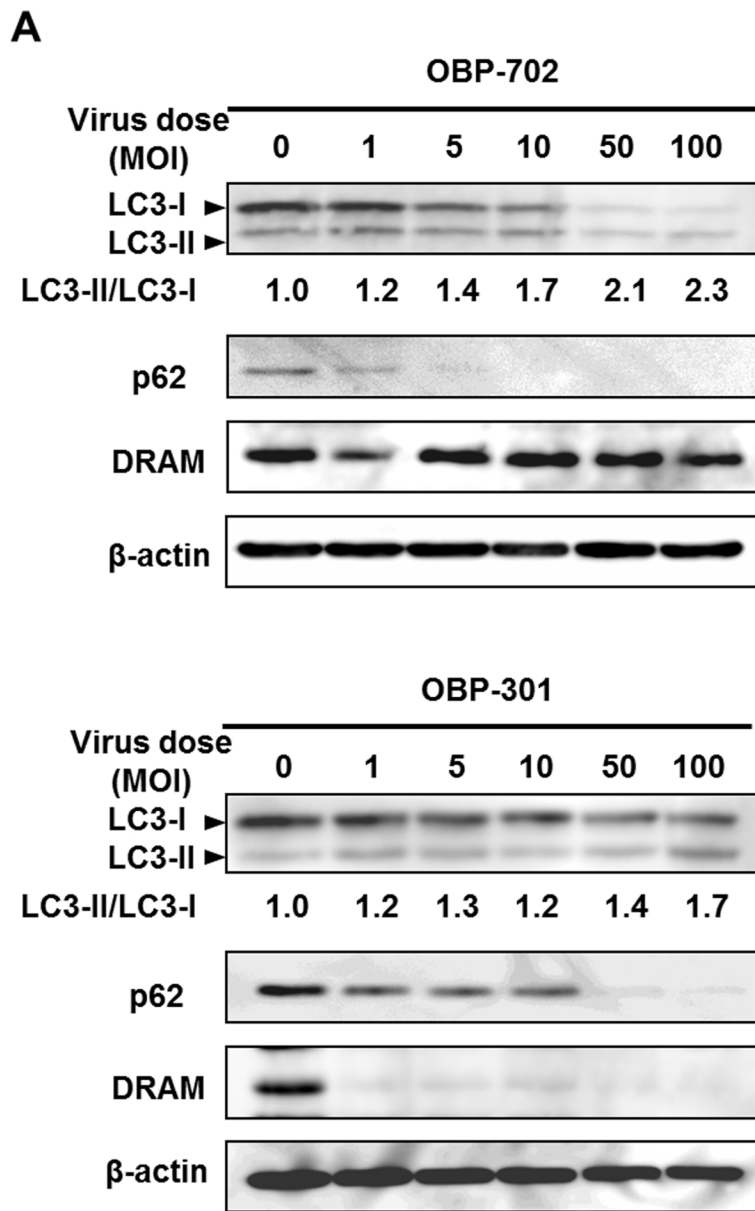


Fig. 4

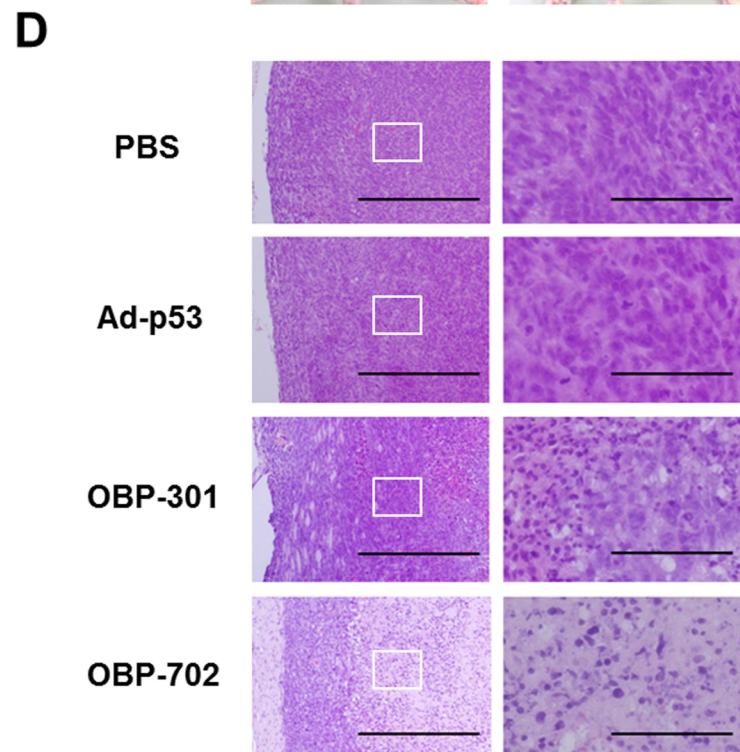
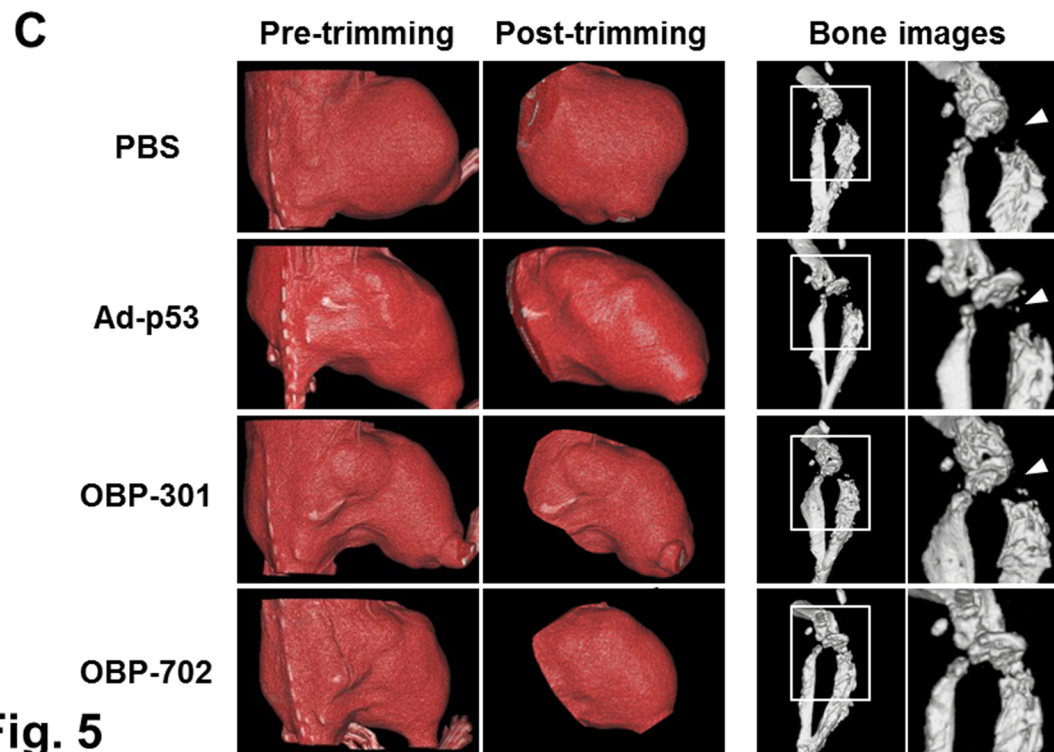
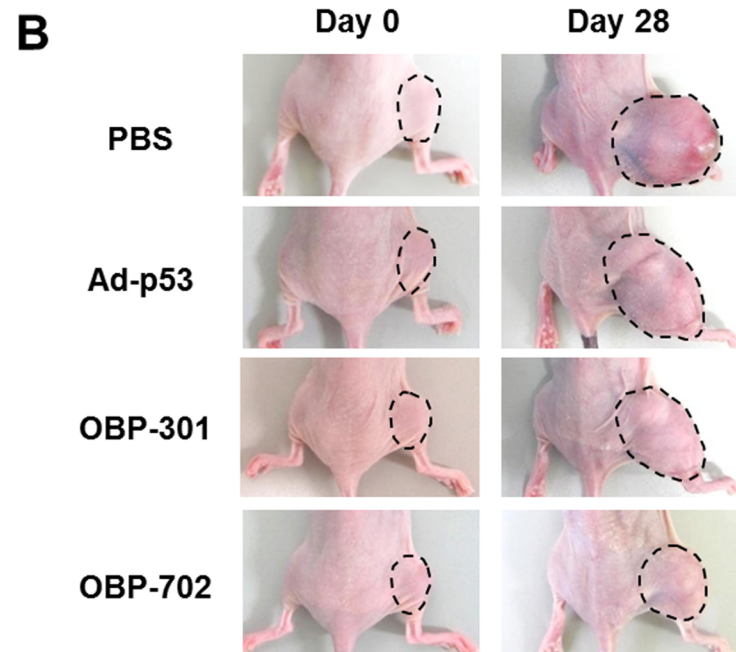
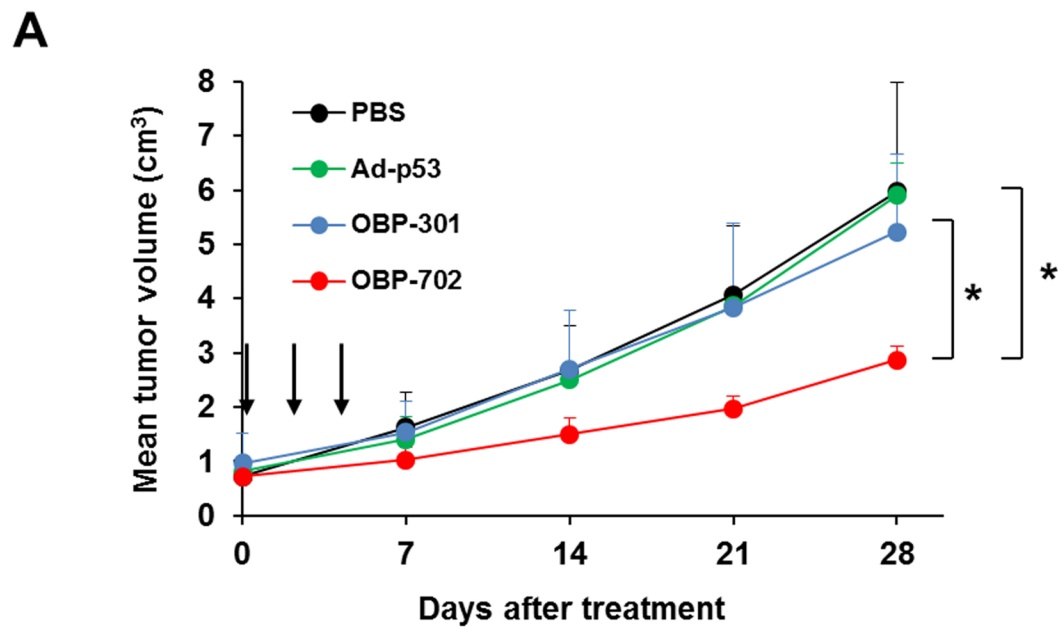


Fig. 5

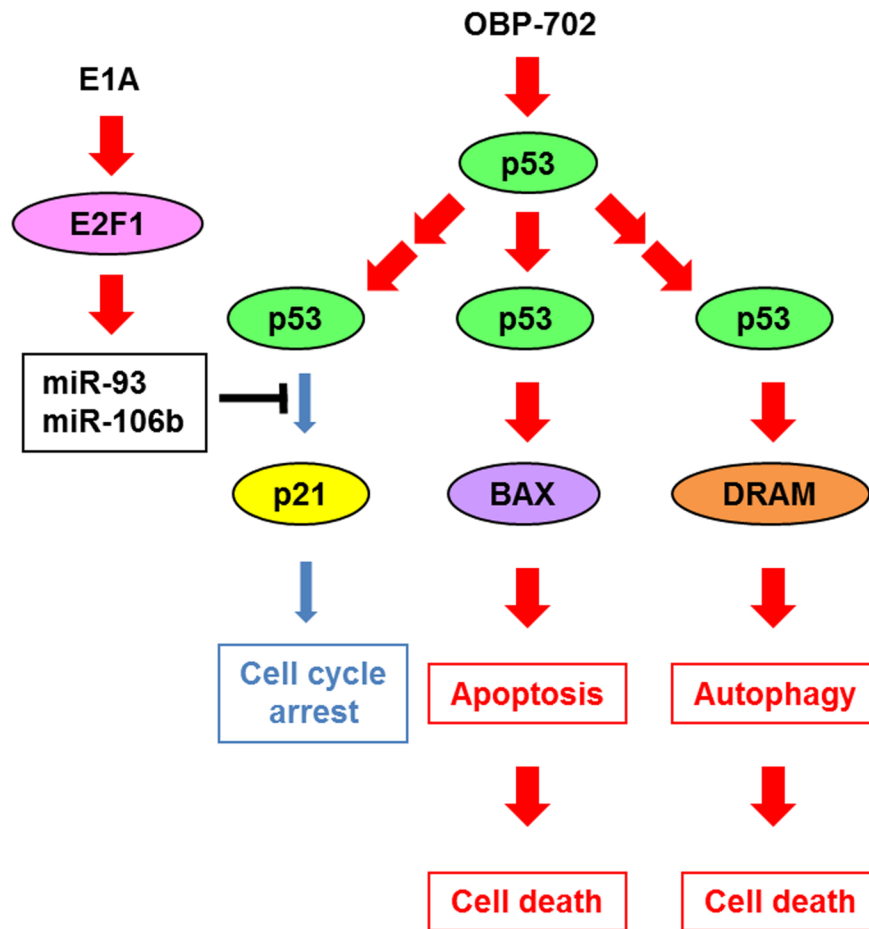


Fig. 6